Spectroscopic Investigation of Al₂N and Its Anion via Negative Ion Photoelectron Spectroscopy

Giovanni Meloni,[†] **Sean M. Sheehan, Bradley F. Parsons, and Daniel M. Neumark***

Department of Chemistry, University of California, Berkeley, California 94720, and Chemical Sciences Division, Lawrence Berkeley National Laboratory, Berkeley, California 94720

Negative ion photoelectron spectroscopy was used to elucidate the electronic and geometric structure of the gaseous Al_2N/Al_2N^- molecules, using photodetachment wavelengths of 416 nm (2.977 eV), 355 nm (3.493 eV), and 266 nm (4.661 eV). Three electronic bands are observed and assigned to the $X^2\Sigma_u^+ \leftarrow X^1\Sigma_g^+$, $A^2\Pi_u \leftarrow X^1\Sigma_g^+$, and $B^2\Sigma_g^+ \leftarrow X^1\Sigma_g^+$ electronic transitions, with the caveat that one or both excited states may be slightly bent. With the aid of density functional theory calculations and Franck−Condon spectral simulations, we determine the adiabatic electron affinity of Al_2N, 2.571 ± 0.008 eV, along with geometry changes upon photodetachment, vibrational frequencies, and excited-state term energies. Observation of excitation of the odd vibrational levels of the antisymmetric stretch (ν_3) suggests a breakdown of the Franck−Condon approximation, caused by the vibronic coupling between the $X^2\Sigma_u^+$ and $B^2\Sigma_g^+$ electronic states through the ν_3 mode.

I. Introduction

In the past decade, much interest has been devoted to cluster science owing to the possibility of synthesizing new materials starting from building blocks, such as clusters. The fascination in producing cluster-assembled materials derives from the fact that they may differ significantly from their crystalline counterparts,[1,2] presenting different optical, mechanical, and electronic properties. An understanding of geometric and electronic structure and stability of small clusters is therefore desirable.

In general, group III nitrides can be used as blue/green light emitters, high-temperature electronic devices, and UV photodetectors.[3,4] Aluminum−nitrogen clusters represent an attractive class of group III nitride compounds to investigate because of their potential use as precursors in the growth of novel materials. While many nitrides of group III elements have been extensively studied in the condensed phase, little is known regarding the spectroscopic properties of their smaller molecular subunits. In this article, we describe the findings for the ground and low-lying electronic states of the Al_2N molecule using negative ion photoelectron (PE) spectroscopy and compare the results with the isovalent B_2N and Ga_2N molecules.[5,6] This investigation represents our continued effort to characterize group III−V molecular clusters[7−13] by anion PE spectroscopy.

Experimental studies on gaseous Al_2N are limited, and no information is available on its electronic spectrum. The first observation of Al_2N was made by Gingerich[14] during the vaporization of a AlN−Au−graphite mixture via Knudsen cell mass spectrometry (KCMS) in the effort to determine its atomization enthalpy. Andrews et al.[15] identified several Al_xN_y species in an infrared matrix isolation experiment of laser-vaporized aluminum with N_2. In particular, they observed two bands at 956.7 and 1501.6 cm⁻¹ that, on the basis of the isotopic ratio and density functional theory (DFT) calculations, were assigned to the antisymmetric stretch (σ_u) and combination band

($\sigma_g + \sigma_u$), respectively, of the linear centrosymmetric Al−N−Al molecule. Nayak et al.[16] produced Al_xN^- clusters by laser ablation of a pure Al disk with a N_2/He carrier gas and measured the anion PE spectra of Al_3N^- and Al_4N^-. Meloni and Gingerich[17] obtained the atomization energy and enthalpy of formation of the Al_2N molecule using KCMS and a new set of molecular parameters computed at the density functional level of theory.

Nayak et al.[18] investigated the evolution of bonding in Al_xN ($x = 1−6$, 12) clusters using DFT calculations, showing that for small clusters with $x \leq 6$ the bonding character is intermediate between ionic, covalent, and metallic for the icosahedral $Al_{12}N$. Moreover, for the Al_2N $X^2\Sigma_u^+$ ground state, they obtained a linear centrosymmetric structure with a bond distance of 1.74 Å. Blanco and co-workers[19,20] performed DFT calculations to study the molecular parameters, stability, ionization energies, and chemical bonding of group III nitride clusters. They found the lowest-energy geometry of Al_2N to have C_{2v} symmetry, nearly degenerate with the linear centrosymmetric structure, with an Al−N bond length of 1.75 Å and an apex angle of 177°. Leskiw et al.[21] carried out DFT calculations to explain the observed mass spectra obtained from a vaporized aluminum rod in the presence of a helium carrier gas and N_2 after reacting the clusters with O_2. Their calculations indicated that both neutral and anionic Al_2N ground states are bent with a bond distance difference between the two of 0.02 Å. However, Leskiw et al.[21] did not perform frequency analyses to verify the stabilities of the optimized geometries. Jiang et al.[22] and Guo et al.,[23] at the Becke three-parameter exchange functional with the Lee, Yang, and Parr correlation functional (B3LYP) with the split-valence diffuse triple-ζ (6-311+G) basis set, found that the neutral Al_2N $^2\Sigma_u^+$ ground state is linear and 40 meV more stable than the C_{2v} $^2B_2$ isomer. The same energy ordering stays for the anion, with the linear structure 3 meV more stable than the bent one.

In this study, we report the first anion PE experiments on Al_2N^- using photodetachment energies of 4.661 (266 nm), 3.493 (355 nm), and 2.980 eV (416 nm). We measured for the first

time the adiabatic electron affinity (EA) of Al_2N and observed its two lowest excited electronic states. The PE spectra of Al_2N show vibrationally resolved features for the first band. Electronic structure calculations and Franck−Condon spectral simulations were performed yielding neutral and anion vibrational frequencies as well as geometric changes that occur upon photodetachment.

II. Experimental Section

The details of the experimental apparatus used in this investigation have been fully described previously.[24,25] Briefly, the experiments were carried out on a tandem time-of-flight (TOF) negative ion photoelectron spectrometer, incorporating a linear reflectron TOF mass spectrometer and a field-free TOF photoelectron analyzer.

Al_2N^- is generated by pulsed laser vaporization of a rotating and translating AlN ceramic disk (>95% dense) with the second harmonic (2.331 eV, 15−20 mJ/pulse) of a pulsed Nd:YAG laser. Nitrogen is used as the carrier gas after passing it through a stainless steel bubbler containing a 14.8 N solution of NH_4-OH (Fisher Scientific). This step helps in reducing the formation of aluminum oxide species after laser ablation, most likely owing to the reaction of ammonia with O_2 to produce water and N_2.

The resulting plume generated by laser ablation was entrained in a pulse of N_2 from a piezoelectric valve and expanded through a 19-mm-long clustering channel. It was then skimmed and entered the first differentially pumped region of a linear reflectron TOF mass spectrometer. The ions formed during the expansion were extracted and accelerated perpendicularly to their flow direction to a beam energy of 2.545 keV. A $m/\Delta m$ resolution of 2000 is achieved.

Mass-selected anions were focused and sent to the interaction region, where they intersected a pulsed laser beam at a wavelength of 416 (2.980 eV), 355 (3.493 eV), or 266 nm (4.661 eV). The photon wavelengths of 355 and 266 nm were obtained by tripling and quadrupling the fundamental of a pulsed fixed-frequency Nd:YAG laser; the 416-nm photon wavelength was generated by Stokes-shifting the third harmonic in a high pressure (325 psig) H_2 Raman cell. Typically, a pulse energy of 1−6 mJ was used. Photoelectrons were detected at the end of a 1-m-long field-free flight tube and energy analyzed by TOF. The electron kinetic energy (eKE) scale was calibrated using the known PE spectra of O_2^- at 355 and 416 nm and Cl^-, Br^-, and I^- at 266 nm. The energy resolution is 8−10 meV at 0.65 eV eKE and degrades as $(eKE)^{3/2}$ at higher energy.

The PE spectra were taken at two laser polarization angles (θ), 0° and 90° with respect to the direction of electron detection. This angle was varied by means of a half-wave plate. The angular distribution of the photodetachment intensity obtained with linearly polarized light is then given by

$$\frac{d\sigma}{d\Omega} = \frac{\sigma_{total}}{4\pi}\left[1 + \frac{\beta(eKE)}{2}(3\cos^2\theta - 1)\right] \quad (1)$$

where σ_{total} is the total photodetachment cross-section, and β-(eKE) is the anisotropy parameter which varies from −1 to +2 and can be calculated using

$$\beta = \frac{I_{0°} - I_{90°}}{(1/2)I_{0°} + I_{90°}} \quad (2)$$

β is characteristic for each neutral ← anion electronic transition and can be used to distinguish between peaks of overlapping transitions.
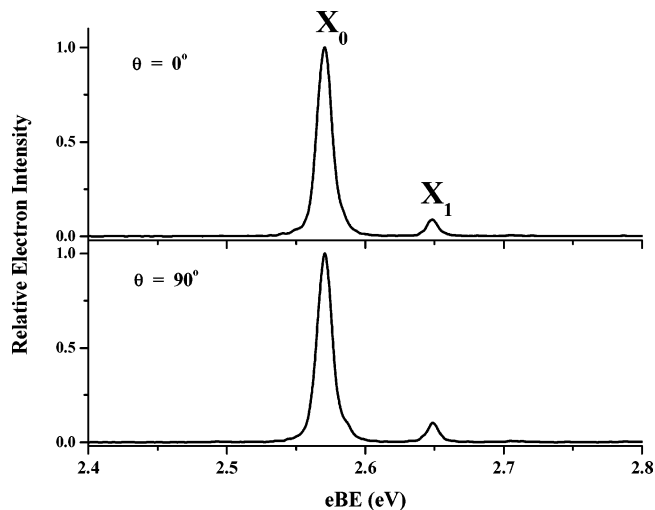

Figure 1. Photoelectron spectra of Al_2N^- at 416 nm photodetachment wavelength taken with $\theta = 0°$ (top) and 90° (bottom).
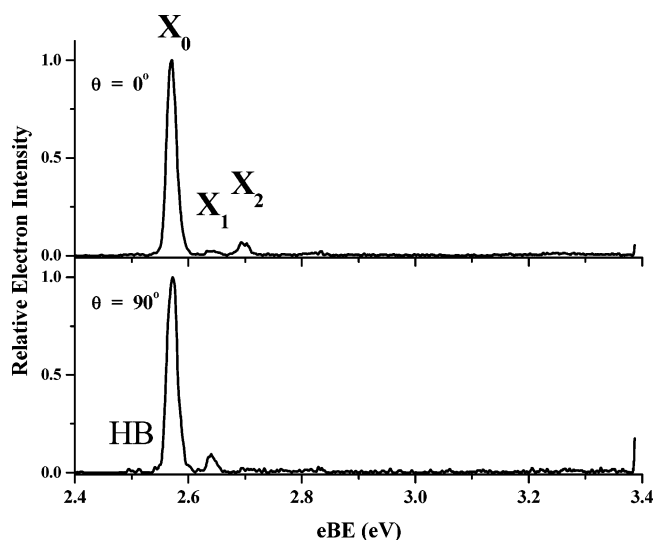

Figure 2. Photoelectron spectra of Al_2N^- at 355 nm photodetachment wavelength taken with $\theta = 0°$ (top) and 90° (bottom).

III. Results

A. Photoelectron Spectra. Figures 1−3 show PE spectra of Al_2N^- taken at photon wavelengths of 416, 355, and 266 nm, respectively, and laser polarization angles θ of 0° and 90°. In these spectra, the PE intensity in relative units is plotted as a function of the electron binding energy (eBE) in electron volts, defined as

$$eBE = h\nu - eKE = EA + E^{(0)} - E^{(-)} \quad (3)$$

where $h\nu$ = 2.980, 3.493, and 4.661 eV are the laser photodetachment energy values, $E^{(0)}$ is the internal energy of the neutral, and $E^{(-)}$ is the internal energy of the anion. The PE spectra comprise electronic transitions to different vibronic states of the neutral, with the lowest-lying state occurring at the lowest eBE.

The 416 nm PE spectra (Figure 1) show two peaks labeled X_0 and X_1, with similar anisotropy parameters, while the 355 nm spectra in Figure 2 comprise three peaks labeled as X_0, X_1, and X_2 with different β values. The 266 nm PE spectra in Figure 3 show two more bands, A and B, in addition to band X. As expected, the resolution of band X degrades as the photon energy, and hence the eKE, increases. Peak positions and
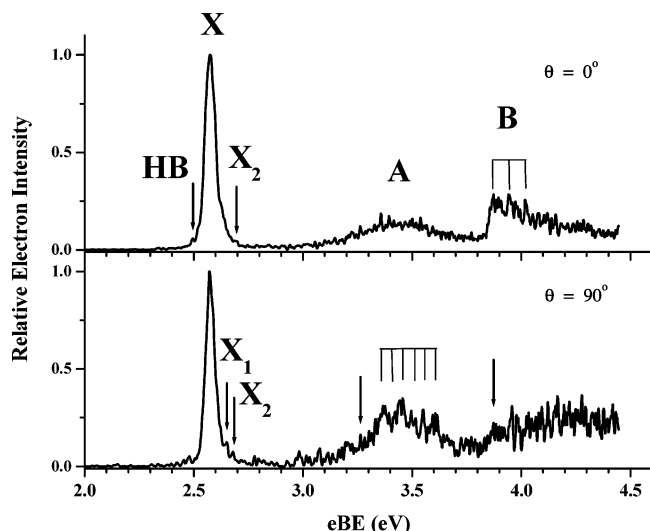
Figure 3. Photoelectron spectra of Al$_2$N$^-$ at 266 nm photodetachment wavelength taken with $\theta = 0°$ (top) and 90° (bottom).

spacings for band X at 416 and 355 nm photodetachment wavelengths are listed in Table 1, along with anisotropy parameters β.

In Figure 1, band X has a strong peak at 2.571 eV (X$_0$) and a much weaker peak (X$_1$) at 2.647 eV. This appears to be a short vibrational progression, with a frequency of 610 cm^{-1}, dominated by the origin transition. The fact that only a single vibrational quantum is excited is characteristic of a small geometry rearrangement upon photodetachment. From our electronic structure calculations (see next section), the ground state of Al$_2$N is X$^2\Sigma_u^+$ and the anion has a X$^1\Sigma_g^+$ electronic ground state. The computed energy required for the X$^2\Sigma_u^+$ + e$^-$ $\leftarrow$ X$^1\Sigma_g^+$ transition is 2.40 eV, very close to the experimental band X origin, and we assign band X to this transition. Taking peak X$_0$ as the vibrational origin yields 2.57 eV for the adiabatic electron affinity of Al$_2$N; this value is refined slightly by the simulations presented in section IV.

The 355 nm spectra in Figure 2 comprise three well-separated peaks. Peaks X$_0$ and X$_1$ have the same eBE as the corresponding peaks in the 416 nm spectrum. However, the β-parameter for peak X$_0$ at 355 nm is considerably more positive than at 416 nm. A new feature, X$_2$, is seen lying 1030 cm^{-1} from X$_0$ and corresponds to excitation of a different vibrational mode of Al$_2$N. The anisotropy parameter for peak X$_2$ is considerably more positive than X$_0$ and X$_1$. A very small spectral feature, labeled HB, is present at 2.51 eV and is assigned to a hot band from an excited vibrational level of the ground state of the anion.

In Figure 3, the 266 nm PE spectrum shows three bands, labeled X, A, and B, two of which, A and B, are not observed in the 416 and 355 nm PE spectra. The vibrational features seen for band X at the two lower photon energies are barely resolved at 266 nm. In the $\theta = 90°$ spectrum, band A shows a partially resolved structure with an approximate vibrational frequency of 400 cm^{-1}. Also, band B shows a partially resolved progression in the $\theta = 0°$ spectrum, indicated by the comb, with a peak spacing of about 580 cm^{-1}. The congested nature of bands A and B prevents a simple and direct determination of their vibrational origins. Moreover, bands A and B are more extended than band X, indicating a relatively large geometry rearrangement upon photodetachment. Band B presents a sharper onset at $\theta = 0°$ than $\theta = 90°$. All the bands are more intense at $\theta = 0°$. The appearance of bands X and A is similar to analogous bands seen in the Ga$_2$N$^-$ PE spectrum.[6] Assignment of these bands is discussed in section IV.

B. Electronic Structure Calculations. To aid in interpreting the PE spectra, electronic structure calculations were performed using the *Gaussian 03* program package.[26] DFT was employed using the B3LYP functional. The Pople-style all-electron split valence and polarization triple-ζ (6-311+G) basis set was used for both Al and N.[27] Optimized geometries, harmonic vibrational frequencies, and energetics (including term energies, T_e, and adiabatic detachment energies, ADE) for the ground and various excited electronic states of Al$_2$N/Al$_2$N$^-$ are summarized in Table 2. The adiabatic detachment energy is defined as the energy difference between the $v = 0$ levels of the anion ground state and neutral electronic state in question and, in the case of the neutral ground state, is equal to the electron affinity. Also, in Table 2, the expectation values for the square of the spin operator ($\langle S^2 \rangle$) are listed for each electronic state; these values indicate minimal spin contamination in all cases.

Our computations yield a similar ordering of electronic states as the work of Wang and Balasubramanian[28] for the isovalent Ga$_2$N molecule, with linear, centrosymmetric $^1\Sigma_g^+$ and $^2\Sigma_u^+$ ground states for the anion and neutral, respectively. No evidence of bent structures for both the anion and the neutral ground states was found. The outer molecular orbital (MO) configurations for the anion and the neutral Al$_2$N ground states are $6\sigma_g^2\ 2\pi_u^4\ 5\sigma_u^2$ and $6\sigma_g^2\ 2\pi_u^4\ 5\sigma_u^1$, respectively. The $5\sigma_u^2$ highest occupied MO (HOMO) is mainly composed of a linear combination of Al s-like and N p$_z$-like orbitals and has slightly antibonding character. Therefore, photodetachment of an electron from the $5\sigma_u^2$ MO should result in somewhat shorter Al$-$N

TABLE 1: Peak Positions (in eV), Peak Spacings (in cm^{-1}), and β Parameters for Band X at different photon wavelengths (nm)

photon wavelength	X$_0$	X$_1$	X$_2$	HB	X$_0$–X$_1$	X$_0$–X$_2$	HB	β_{X_0}	β_{X_1}	β_{X_2}
416	2.571	2.647			610			0.2	0.1	
355	2.570	2.644	2.698	2.505	600	1030	520	0.9	0.2	1.5

TABLE 2: Computed Optimized Molecular Parameters (r_{Al-N} in Å and ν in cm^{-1}), Zero-Point Energy Vibrational Energies (ZPE in eV), Term Energies (T_e in cm^{-1}), Adiabatic Detachment Energies (ADE in eV), and $\langle S^2 \rangle$ at the B3LYP/6-311+G Level of Theory

molecule	state	r_{Al-N}	$\nu_1{}^a$	ν_2	ν_3	ZPE	T_e	ADE	$\langle S^2 \rangle$
Al$_2$N$^-$	X$^1\Sigma_g^+$	1.765	499	177	1117	0.12			
	a$^3\Pi_g$	1.770	479	169, 172^b	2344	0.20	20490		2.012
Al$_2$N	X$^2\Sigma_u^+$	1.750	505	175	1040	0.12		2.40	0.757
	A$^2\Pi_u$	1.880	401	95, 166^b	865	0.09	4890	3.01	0.755
	B$^2\Sigma_g^+$	1.724	559	583	1511	0.20	10860	3.75	0.756

^{a} ν_1 is the symmetric stretching (σ_g), ν_2 the bending (π), and ν_3 the antisymmetric stretching (σ_u) mode. ^{b} The bending modes of the $^2\Pi_u$ state are not degenerate, for the calculations fail in reproducing the proper cylindrical symmetry.

bonds. In fact, the B3LYP/6-311+G optimized geometries show the Al−N bond length to decrease by 0.015 Å upon photo-detachment.

The $A^2\Pi_u$ state is calculated to be 0.61 eV (4890 cm^{-1}) above the ground electronic state of Al_2N. Its outer MO configuration is found to be $6\sigma_g^2\ 2\pi_u^3\ 5\sigma_u^2$ with the $2\pi_u^3$ MO mainly composed of N p_x-like or p_y-like orbital linear combinations with bonding character. Removal of an electron from the $2\pi_u^3$ MO weakens the Al−N bond, and its calculated value is 0.115 Å longer than r_{Al-N} for the $X^1\Sigma_g^+$ state. All three calculated vibrational frequencies are lower in the $A^2\Pi_u$ state than in the anion, reflecting the smaller Al−N force constants associated with weakening the two bonds.

The $B^2\Sigma_g^+$ state is computed to lie 1.35 eV (10 860 cm^{-1}) higher than the $X^2\Sigma_u^+$ state with an outer MO configuration of $6\sigma_g^1\ 2\pi_u^4\ 5\sigma_u^2$. The $6\sigma_g^1$ MO has an antibonding character and is mainly made of Al s-like and N s-like orbitals. The calculated shortening of the bond distance for the $B^2\Sigma_g^+$ state, 0.041 Å, is consistent with its antibonding character. While all three calculated vibrational frequencies for the $B^2\Sigma_g^+$ state are larger than in the anion, the bend frequency increases by greater than a factor of 3, indicating a much more rigid linear structure than in the anion. This is also supported by a simple "bond-order" scheme. In fact, giving to the $5\sigma_u$ MO a nonbonding character, we would obtain a bond order of 1 for the $Al_2N^-\ X^1\Sigma_g^+$ and $Al_2N\ X^2\Sigma_u^+$ states, 0.75 for the $Al_2N\ A^2\Pi_u$ state, and 1.25 for the $Al_2N\ B^2\Sigma_g^+$ state. The higher bend mode for the $^2\Sigma_g^+$ electronic state can be then explained in terms of a multiple bond character.

IV. Discussion

Analysis and assignment of the electronic transitions and vibrational progressions in Figures 1−3 are facilitated by comparison with the electronic structure calculations described in the previous section. The B3LYP/6-311+G energetics suggest an assignment of band X to the $X^2\Sigma_u^+ \leftarrow X^1\Sigma_g^+$ transition, band A to the $A^2\Pi_u \leftarrow X^1\Sigma_g^+$ transition, and band B to the $B^2\Sigma_g^+ \leftarrow X^1\Sigma_g^+$ transition. The calculated changes in bond length would lead one to expect a very short vibrational progression for band X, with more extended progressions for bands A and B, in agreement with experiment. On the other hand, bands A and B are rather congested for transitions between linear, centrosymmetric anion and neutral states. The observed vibrational progressions listed in Table 1 are analyzed and compared with the simulation values hereafter.

To investigate our assignments further, spectral simulations of bands X, A, and B were carried out within the Franck−Condon (FC) approximation assuming harmonic oscillator potentials.[29] We used the B3LYP/6-311+G force constants and optimized geometries for the initial state of the anion and the final state of the neutral to determine the normal coordinate displacement. The normal mode changes for the considered electronic transitions, computed harmonic vibrational frequencies, and transition origins were used as initial conditions for the simulations and were adjusted to reproduce the experimental PE spectra. The anion vibrational temperature used is 300 K for the 416 nm and 400 K for the 266 nm PE spectra. The FC simulations are particularly important for the origin assignment of broad bands comprising extended progressions. The optimized parameters are listed in Table 3, and the FC simulated PE spectra are shown in Figure 4.

Since the first calculated excited electronic state of Al_2N^-, $a^3\Pi_g$, is 2.54 eV above the ground state, it is safe to assume that all the transitions observed are from the $X^1\Sigma_g^+$ state. At

TABLE 3: Optimized Parameters for the Al$_2$N Molecule Obtained from the FC Simulation of the PE Spectra[a]

band	state	$\nu_1^{(-)}$	$\nu_1^{(0)}$	ΔQ_1	$|\Delta r_{Al-N}|$	ADE	T
X	$X^2\Sigma_u^+$	520	600	0.105	0.014	2.571	300
		(60)	(40)		(0.010)	(0.008)	
A	$A^2\Pi_u$	520	400	0.870	0.118	3.26	400
		(60)	(80)		(0.020)	(0.12)	
B	$B^2\Sigma_g^+$	520	580	0.360	0.049	3.87	400
		(60)	(60)		(0.020)	(0.12)	

[a] The vibrational modes are in cm^{-1}, the normal mode displacements ΔQ_1 in amu$^{1/2}$ Å, the equilibrium bond distance change Δr_{Al-N} in Å, the ADE in eV, and the anion vibrational temperature T in K. The values in parentheses represent the error.

416 nm, only two peaks are observed. Peak X_0 is the band origin, yielding the adiabatic EA for Al_2N of 2.571 ± 0.008 eV. The X_0-X_1 spacing is fit with the totally symmetric σ_g mode of 600 ± 40 cm^{-1}, higher than the B3LYP/6-311+G value of 505 cm^{-1}, and 75 cm^{-1} higher than the experimental value obtained by Andrews et al.[15] in a cryogenic matrix from the difference of the combination band $(\sigma_g + \sigma_u)$ at 1501.6 cm^{-1} and σ_u at 956.7 cm^{-1}. From the normal mode displacement ΔQ_1 of 0.105 amu$^{1/2}$ Å, we determine the magnitude, $|\Delta r_{Al-N}|$, of the bond distance change between the anion and the neutral upon photodetachment. This value is determined as 0.014 Å, in excellent agreement with the computed $|\Delta r_{Al-N}|$ of 0.015 Å. On the basis of the DFT calculations, the sign is expected to be negative.

The 355 nm spectra present three peaks with different β values. Peak X_1 clearly represents the same transition as at 416 nm, to the $\nu_1 = 1$ level. Comparison of the X_0-X_2 splitting, 1030 cm^{-1}, to the calculated frequencies in Table 2 indicates that peak X_2 is the transition to the ν_3 antisymmetric stretch (σ_u) fundamental in the neutral. Within the FC approximation, only transitions with the $\Delta \nu = 0, \pm 2, \pm 4, ...$ selection rule are allowed for a nontotally symmetric mode. Hence, the observation of peak X_2 indicates a breakdown of the FC approximation. A similar result was attained for the isovalent B_2N molecule[5] and was attributed to vibronic coupling between the $X^2\Sigma_u^+$ and $A^2\Sigma_g^+$ states induced by the σ_u antisymmetric stretch mode. For Al_2N, the $B^2\Sigma_g^+$ state, seen at 266 nm, has the correct symmetry for this vibronic coupling mechanism, in which case σ_u vibrational levels in the $X^2\Sigma_u^+$ are coupled to σ_g levels in the $^2\Sigma_g^+$ state. The partially resolved vibrational structure associated with the $B^2\Sigma_g^+$ state, most likely a symmetric stretch progression (see below), is most prominent at $\theta = 0°$ (Figure 3), as is peak X_2 at 355 nm, so the PE angular distributions, to the extent that they can be compared at different photodetachment wavelengths, are consistent with the proposed vibronic coupling mechanism. A small hot band feature appears at 2.505 eV in Figure 2, assigned to the symmetric stretch of the Al_2N^- ground state of 520 cm^{-1}, since it matches the computed ν_1 frequency for the $X^1\Sigma_g^+$ state of Al_2N^-.

While peak X_2 is clearly present in the 355 nm spectrum, it is absent in the PE spectrum at 416 nm even though it is energetically accessible at that wavelength. It appears that the vibronic coupling effects which cause peak X_2 to have any intensity at all are stronger at the higher photodetachment energy. The wavelength dependence of peak X_2 may reflect the influence of an excited anion electronic state at the higher energy that in some way enhances the vibronic coupling, but it is fair to say that this result is not completely understood at present.

Both the $A^2\Pi_u$ and $B^2\Sigma_g^+$ states are accessed at 266 nm. The extended nature of these bands, combined with the incomplete resolution of vibrational structure in each band, makes it possible
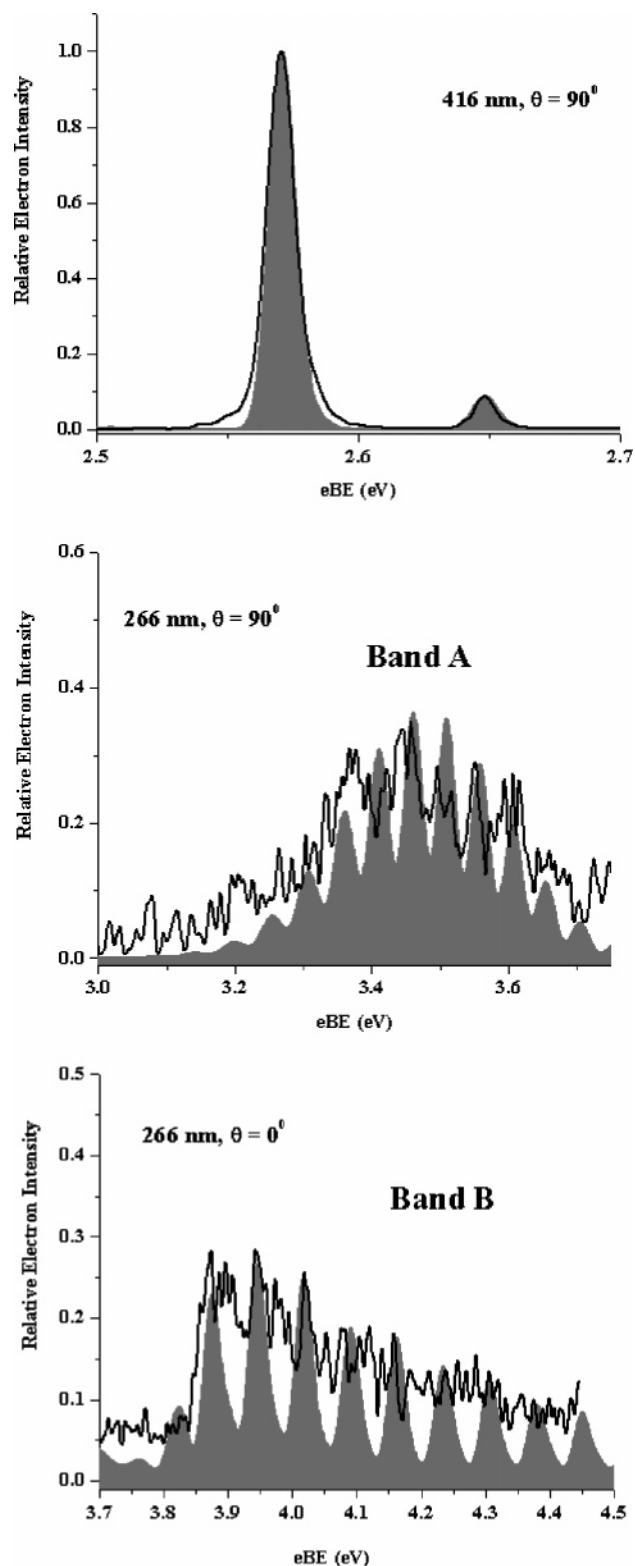
Figure 4. Franck−Condon spectral simulations of Al$_2$N$^-$ PE spectra (gray area) superimposed on the experimental 416 and 266 nm spectra.

to fit each band with more than one set of simulation parameters, involving, for example, different combinations of normal coordinate displacements and excited-state term energies. We thus fit both bands under the restriction that the normal coordinate displacement from the DFT calculation was varied as little as possible in the simulation; this restriction then fixes the term energy even if a clear vibrational origin is not apparent.

The two lone arrows in Figure 3 represent the estimated vibronic origins for the transitions to the A and B excited electronic states.

Band A comprises an extended progression with a partially resolved progression of approximately 400 cm^{-1}, which is close to the calculated symmetric stretch progression of the A$^2\Pi_u$ state. The best-fit simulation, shown in Figure 4, using the parameters in Table 3, is less than perfect but does reproduce the extent of the band and at least some of the vibrational structure. The change in bond length used in this simulation, 0.118 Å, is very close to the calculated increase in bond length of 0.115 Å upon photodetachment to the A$^2\Pi_u$ state. The origin of this band is determined from the FC simulations to be eBE = 3.26 ± 0.12 eV, with the uncertainty reflecting the absence of a clear vibronic origin. This value yields the term energy of 0.69 ± 0.12 eV (5570 ± 970 cm^{-1}) for the A$^2\Pi_u$ electronic state. The B3LYP T_e value of 4890 cm^{-1} (Table 2) lies within this range.

By applying a similar procedure to band B, we find the B$^2\Sigma_g^+$ state origin to be at eBE = 3.87 ± 0.12 eV. This value yields a term energy for the B$^2\Sigma_g^+$ state of 1.30 ± 0.12 eV (10 490 ± 970 cm^{-1}), in good agreement with the computed B3LYP T_e value. The normal mode displacement for the symmetric stretch mode is 0.360 amu$^{1/2}$ Å, corresponding to a bond distance change of 0.049 Å, in good agreement with the negative computed Δr_{Al-N} of 0.041 Å. There is a partially resolved vibrational feature of approximately 580 cm^{-1} assumed to be the σ_g mode of the B$^2\Sigma_g^+$ state for the FC simulation; this value is close to the calculated frequency, 559 cm^{-1}. The simulation also includes small contributions from even $\Delta\nu$ transitions in the bending mode, whose frequency is calculated to increase dramatically upon photodetachment to the B$^2\Sigma_g^+$ state. As with band A, agreement with the simulation is imperfect; it is possible that there is some activity in the σ_u mode owing to vibronic coupling with σ_g vibrational levels of the X$^2\Sigma_u^+$ state, but there is no direct evidence for such coupling.

While our assignments of bands A and B seem reasonable in light of the reasonable agreement between the experimental and theoretical energetics and geometry changes needed to fit the extent of the bands, the congested nature of bands A and B is unusual for a symmetric, triatomic species. In the case of band A, we have neglected spin−orbit splitting of the A$^2\Pi_u$ state in our simulations, which would certainly increase spectral congestion within this band. An extended progression in the low bend frequency of this state, calculated to be around 100 cm^{-1}, would be difficult to resolve but should not be present for a linear−linear photodetachment transition. However, if the A state were slightly bent, one would expect bend and symmetric stretch progressions in the PE spectra. Comparison of band B in the $\theta = 0°$ and 90° spectra suggests there may be a broad feature underlying the partially resolved structure seen at $\theta = 0°$, possibly due to yet another electronic state with a very different geometry from the anion. More sophisticated electronic structure calculations on the excited states of Al$_2$N would be highly desirable in formulating a more complete picture of the PE spectra.

Finally, we compare the results for Al$_2$N$^-$/Al$_2$N with those for the isovalent B$_2$N$^-$/B$_2$N and Ga$_2$N/Ga$_2$N$^-$.[5,6] The EA of B$_2$N, 3.098 ± 0.005 eV, is 0.527 eV higher than EA(Al$_2$N) determined in this study. In the B$_2$N investigation, two electronic states were accessed at 266 nm, the X$^2\Sigma_u^+$ and A$^2\Sigma_g^+$ states, whereas here with the same photon energy, three electronic transitions were observed, yielding the determination of the energy separation between the neutral ground state and the first two excited states of Al$_2$N. The Al$_2$N$^-$ PE spectrum more

closely resembles that of Ga_2N^-, which comprises two bands clearly analogous to bands X and A seen here, and for which the same electronic state assignments were made, with the caveat that band A might represent a transition to a bent neutral state. The EA of Ga_2N, 2.506 eV, is also very close to that of Al_2N. No analogue to band B was seen in the Ga_2N^- spectrum, however, even at considerably higher photon energy (5.82 eV). All three species show evidence for excitation of odd quanta of the σ_u mode in the $X^2\Sigma_u^+$ ground state via vibronic coupling between $^2\Sigma_u^+$ and $^2\Sigma_g^+$ states.

Conclusions

PE spectra of Al_2N^- taken at 416, 355, and 266 nm photon wavelengths have been presented. With the aid of DFT calculations, we analyzed the spectra. The three observed electronic bands were assigned to photodetachment between linear, centrosymmetric structures of the anion and the neutral, specifically from the anion $X^1\Sigma_g^+$ ground state to the ground $X^2\Sigma_u^+$ and first two excited $A^2\Pi_u$ and $B^2\Sigma_g^+$ states of the neutral, but it is possible that one or both excited states is bent. The adiabatic EA of Al_2N is reported as 2.571 ± 0.008 eV. Moreover, from the spectral Franck–Condon simulations, geometry changes and vibrational frequencies were obtained. From the band origins, we determined the term energies for the first two excited states that were not previously reported. The ground-state band shows evidence for vibronic coupling between the $X^2\Sigma_u^+$ and $B^2\Sigma_g^+$ neutral states via the ν_3 antisymmetric stretch. Simulations of the excited-state bands were only partially successful, suggesting the need for further experimental and theoretical work.

References and Notes

(1) Jena, P.; Khanna, S. N.; Rao, B. K. *Surf. Rev. Lett.* **1996**, *3*, 993.

(2) Castleman, A. W.; Bowen, K. H. *J. Phys. Chem.* **1996**, *100*, 12911.

(3) Morkoc, H.; Strite, S.; Gao, G. B.; Lin, M. E.; Sverdlov, B.; Burns, M. *J. Appl. Phys.* **1994**, *76*, 1363.

(4) Ponce, F. A.; Bour, D. P. *Nature* **1997**, *386*, 351.

(5) Asmis, K. R.; Taylor, T. R.; Neumark, D. M. *J. Chem. Phys.* **1999**, *111*, 8838.

(6) Sheehan, S. M.; Meloni, G.; Parsons, B. F.; Wehres, N.; Neumark, D. M. *J. Chem. Phys.* **2006**, *124*, 064303.

(7) Xu, C. S.; Debeer, E.; Arnold, D. W.; Arnold, C. C.; Neumark, D. M. *J. Chem. Phys.* **1994**, *101*, 5406.

(8) Arnold, C. C.; Neumark, D. M. Study Of In2p/In2p- and Inp2/Inp2- Using Negative Ion Zero Electron Kinetic Energy Spectroscopy. *Can. J. Phys.* **1994**, *72*, 1322.

(9) Asmis, K. R.; Taylor, T. R.; Neumark, D. M. *Chem. Phys. Lett.* **1998**, *295*, 75.

(10) Asmis, K. R.; Taylor, T. R.; Neumark, D. M. *J. Chem. Phys.* **1999**, *111*, 10491.

(11) Taylor, T. R.; Gomez, H.; Asmis, K. R.; Neumark, D. M. *J. Chem. Phys.* **2001**, *115*, 4620.

(12) Gomez, H.; Taylor, T. R.; Neumark, D. M. *J. Phys. Chem. A* **2001**, *105*, 6886.

(13) Gomez, H.; Taylor, T. R.; Zhao, Y.; Neumark, D. M. *J. Chem. Phys.* **2002**, *117*, 8644.

(14) Gingerich, K. A. *J. Chem. Soc. D* **1970**, 441.

(15) Andrews, L.; Zhou, M. F.; Chertihin, G. V.; Bare, W. D.; Hannachi, Y. *J. Phys. Chem. A* **2000**, *104*, 1656.

(16) Nayak, S. K.; Rao, B. K.; Jena, P.; Li, X.; Wang, L. S. Observation of a spin-protected high-energy isomer of Al_4N^- cluster. In *Chem. Phys. Lett.* **1999**, *301*, 379.

(17) Meloni, G.; Gingerich, K. A. *J. Chem. Phys.* **2000**, *113*, 10978.

(18) Nayak, S. K.; Khanna, S. N.; Jena, P. *Phys. Rev. B* **1998**, *57*, 3787.

(19) Kandalam, A. K.; Pandey, R.; Blanco, M. A.; Costales, A.; Recio, J. M. *J. Phys. Chem. B* **2000**, *104*, 4361.

(20) Costales, A.; Kandalam, A. K.; Pendas, A. M.; Blanco, M. A.; Recio, J. M.; Pandey, R. *J. Phys. Chem. B* **2000**, *104*, 4368.

(21) Leskiw, B. D.; Castleman, A. W.; Ashman, C.; Khanna, S. N. *J. Chem. Phys.* **2001**, *114*, 1165.

(22) Jiang, Z. Y.; Ma, W. J.; Wu, H. S.; Jin, Z. H. *THEOCHEM* **2004**, *678*, 123.

(23) Guo, L.; Wu, H. S.; Jin, Z. H. *THEOCHEM* **2004**, *677*, 105.

(24) Metz, R. B.; Weaver, A.; Bradforth, S. E.; Kitsopoulos, T. N.; Neumark, D. M. *J. Phys. Chem.* **1990**, *94*, 1377.

(25) Xu, C. S.; Burton, G. R.; Taylor, T. R.; Neumark, D. M. *J. Chem. Phys.* **1997**, *107*, 3428.

(26) Frisch, M. J.; Trucks, G. W.; Schlegel, H. B.; Scuseria, G. E.; Robb, M. A.; Cheeseman, J. R.; Montgomery, J. A., Jr.; Vreven, T.; Kudin, K. N.; Burant, J. C.; Millam, J. M.; Iyengar, S. S.; Tomasi, J.; Barone, V.; Mennucci, B.; Cossi, M.; Scalmani, G.; Rega, N.; Petersson, G. A.; Nakatsuji, H.; Hada, M.; Ehara, M.; Toyota, K.; Fukuda, R.; Hasegawa, J.; Ishida, M.; Nakajima, T.; Honda, Y.; Kitao, O.; Nakai, H.; Klene, M.; Li, X.; Knox, J. E.; Hratchian, H. P.; Cross, J. B.; Bakken, V.; Adamo, C.; Jaramillo, J.; Gomperts, R.; Stratmann, R. E.; Yazyev, O.; Austin, A. J.; Cammi, R.; Pomelli, C.; Ochterski, J. W.; Ayala, P. Y.; Morokuma, K.; Voth, G. A.; Salvador, P.; Dannenberg, J. J.; Zakrzewski, V. G.; Dapprich, S.; Daniels, A. D.; Strain, M. C.; Farkas, O.; Malick, D. K.; Rabuck, A. D.; Raghavachari, K.; Foresman, J. B.; Ortiz, J. V.; Cui, Q.; Baboul, A. G.; Clifford, S.; Cioslowski, J.; Stefanov, B. B.; Liu, G.; Liashenko, A.; Piskorz, P.; Komaromi, I.; Martin, R. L.; Fox, D. J.; Keith, T.; Al-Laham, M. A.; Peng, C. Y.; Nanayakkara, A.; Challacombe, M.; Gill, P. M. W.; Johnson, B.; Chen, W.; Wong, M. W.; Gonzalez, C.; Pople, J. A. *Gaussian 03*, revision C.02; Gaussian, Inc.: Wallingford, CT, 2004.

(27) Francl, M. M.; Pietro, W. J.; Hehre, W. J.; Binkley, J. S.; Gordon, M. S.; Defrees, D. J.; Pople, J. A. *J. Chem. Phys.* **1982**, *77*, 3654.

(28) Wang, C. S.; Balasubramanian, K. *Chem. Phys. Lett.* **2005**, *402*, 294.

(29) Gomez, H. Ph.D. Thesis, University of California, Berkeley, California, 2002.